AGU PUBLICATIONS

Geophysical Research Letters

RESEARCH LETTER
10.1002/2013GL058683

Key Points:
- Hydromechanical-seismic model is applied to study fracture deformation
- Volumetric deformation of fracture is affected by its geological properties
- Fracture roughness affect its transport and seismic source responses

Correspondence to:
V. Alvarado,
valvarad@uwyo.edu

Citation:
Raziperchikolaee, S., V. Alvarado, and S. Yin (2014), Effect of fracture roughness on seismic source and fluid transport responses, *Geophys. Res. Lett.*, *41*, 1530–1536, doi:10.1002/2013GL058683.

Received 12 NOV 2013
Accepted 24 JAN 2014
Accepted article online 28 JAN 2014
Published online 12 MAR 2014

Effect of fracture roughness on seismic source and fluid transport responses

S. Raziperchikolaee[1], V. Alvarado[1], and S. Yin[1]

[1]Department of Chemical and Petroleum Engineering, University of Wyoming, Laramie, Wyoming, USA

Abstract To explain how fracture roughness affects seismic source and transport response of deformed fractured rock, we developed a microscale fluid flow-geomechanics-seismicity model. The modeling method considers comprehensive grains and cement interactions. Fluid flow behavior is obtained through realistic network models of the pore space in the compacted assembly. In addition, forces and displacements in the grains involved in the bond breakage are measured to determine seismic moment tensor. The results of our work show that in addition to stress conditions in the target formation, geological properties of preexisting fractures affect volumetric deformation of the seismic source as well. The results of the model proves that roughness of fractures, applied in a Berea sample, causes deviation of source mechanism of acoustic emission events toward opening tensile part and enhances the permeability of the sample significantly during its failure even under confining pressure.

1. Introduction

Moment tensor solution is an approach to study complex mechanisms involved in rock fracturing. With nonzero volumetric deformation of a seismic source considered, the moment tensor represents all types of crack propagation that have contribution to rock damage [*Aki and Richards*, 2002]. Characterizing source mechanism of induced seismicity by moment tensor inversion [*Baig and Urbancic*, 2010] reveals that microearthquakes with volumetric components have been found in different environments [*Miller et al.*, 1998]. Tensile microearthquakes were recorded at volcanic and geothermal areas under high fluid pressure [*Julian et al.*, 2010]. In addition, microearthquakes with volumetric component could be induced during hydraulic stimulation operation intended to increase permeability in oil and gas reservoirs [*Šílenỳ et al.*, 2009]. Volumetric changes related to microseismic events are a function of combined shear and tensile forces in the source of events. In a recent work, *Fischer and Guest* [2011] showed that the presence of tensile deformation in the source of microseismic events depends on differential stress along the preexisting fracture exhibiting failure tendency.

While it is proven that geomechanical conditions could cause volumetric deformation in the source of microseismic events, the impact of geological properties of fractures on generating events with tensile component has been neglected. In this sense, could fracture roughness affect volumetric deformation in the source of event? Conversely, is its effect on seismic source and transport response of deformed fracture significant? In our research, a microscale hydromechanical-seismic model has been developed to address effects of fracture roughness on fluid flow and seismic source behavior of deformed fractured samples. By modeling pore structure between grains realistically, we are able to predict fluid flow behavior of the rock sample under different stress conditions. In addition, forces and displacements around microcracks are investigated to determine seismic source behavior of microfractures. A fractured Berea sandstone sample is simulated based on its geological and geomechanical properties. The roughness of fracture is modeled by assigning dilation angle and asperity on the grains involved in the fracture. The simulation results show that sources of acoustic emission (AE) events generated during deformation of rough fractures have volumetric component toward tensile crack opening, in contrast to smooth plane fractures. In addition, permeability of the rock sample with a rough fracture enhances significantly during its failure under confining pressure in the numerical triaxial tests.

2. Numerical Model

2.1. Microscale Geomechanical Behavior Modeling

In microscale modeling of rocks, constitutive elements such as grains, cracks, and pores are explicitly modeled, enabling us to better understand rock mechanical behavior. The bonded particle model (BPM)

represents the rock as a compacted bonded assembly of rigid particles interacting at soft contacts and can be used to predict macroscopic rock behavior from micromechanical properties. BPM can also model and track damage formation inside a rock sample due to progressive development and coalescence of microcracks to predict failure behavior of rocks [*Potyondy and Cundall*, 2004].

2.2. Modeling Fluid Flow Behavior at Microscale

An accurate representation of pore space is needed to predict fluid flow behavior in sedimentary rocks. To study the effect of rock deformation on transport properties, we build a dynamic pore network model regenerated as a function of grain deformation. To construct the network of pores and pipes, tetrahedral cells are made by grouping nearest four neighbor particles together in the rock sample. Cell interior corresponds to the pore, and the location of each pore is the geometric center of the cell. The cell face corresponds to the pipe and represents the flow path between two adjacent connected pores. Conductivity of pipes is the main parameter used to calculate permeability of the network. The length of the pipe is the distance between pores, and the effective radius of each cylindrical pipe is calculated as an average of two radii [*Bryant et al.*, 1993]. The first radius, r_c, corresponds to the largest circle that can be inscribed in the cross section among three particles. The second radius, r_e, corresponds to the equivalent circle radius with the same total area as the cross section among three particles. Since the inscribed circle always covers a smaller area than the cross section, a cylindrical tube of radius r_c has lower hydraulic conductivity than the conduit. On the other hand, a circle is the most efficient cross section for fluid flow, a cylindrical tube of radius of r_e has larger conductivity than a conduit. r_{eff} is bounded by these two radii. The schematic of the radii used to calculate effective radius of each pipe is shown in Figure 1a.

The Hagen-Poiseuille law is used for calculation of hydraulic conductance of each pipe.

$$g_{ij} = \frac{\pi r_{\text{eff}}^4}{\mu 8z} \tag{1}$$

where g is the hydraulic conductance, r_{eff} and z are the effective radius and length, and μ is the fluid viscosity. Steady state pressure distribution is applied in the network by calculating flow through each pipe and solving the resulting set of equations representing mass conservation to measure permeability of network. By applying the steady state pressure distribution and assuming the instantaneous response of an incompressible fluid, effects of fluid pressure on further rock deformation are not considered for calculation of rock permeability. Effect of pore pressure decrement due to rock expansion on further deformation is a complicated function of initial permeability of sample, pore pressure inside it, and geological properties of sample, which is not considered in our work. In our hydromechanical model, the one-way coupling occurs through geometrical constrains of pore structure of the sample in each time step as a function of rock deformation. To calculate the permeability of the sample, pressure boundary conditions are applied to the inlet and outlet sections of the sample as to estimate pressure inside the sample. Zero-flux condition is imposed on the remaining boundaries along the main direction of flow.

2.3. Modeling of Seismic Source Deformation

AE data provide valuable information to study the mechanics of microcrack generation and coalescence leading to developing of the macrofracture in the rock sample [*Lockner et al.*, 1991]. By measuring the forces in the contacts around the source particles and the distance between the contact location and the centroid of an AE event, and by considering microcracks that develop close together in space and time as one event, seismic moment of AE events can be calculated to study the complex behavior of mechanisms involved in fracturing in detail [*Hazzard and Young*, 2002].

In this letter, components of unbalanced forces developed in the source particles and concentrated in the particle center are measured at each time step of crack development. By measuring the distance between the contact where bond breakage occurred and the particle center involved in the bond breakage as well, the components of the moment tensor of each microcrack are calculated. The summation of different components of moment tensor of the microcracks that make up one AE event is used to calculate moment tensor of the whole event. Components of moment tensor for an event consist of a cluster of microcracks, calculated as follows:

$$M_{ij} = \sum_{k=1}^{N} F_i^k * R_j^k \tag{2}$$

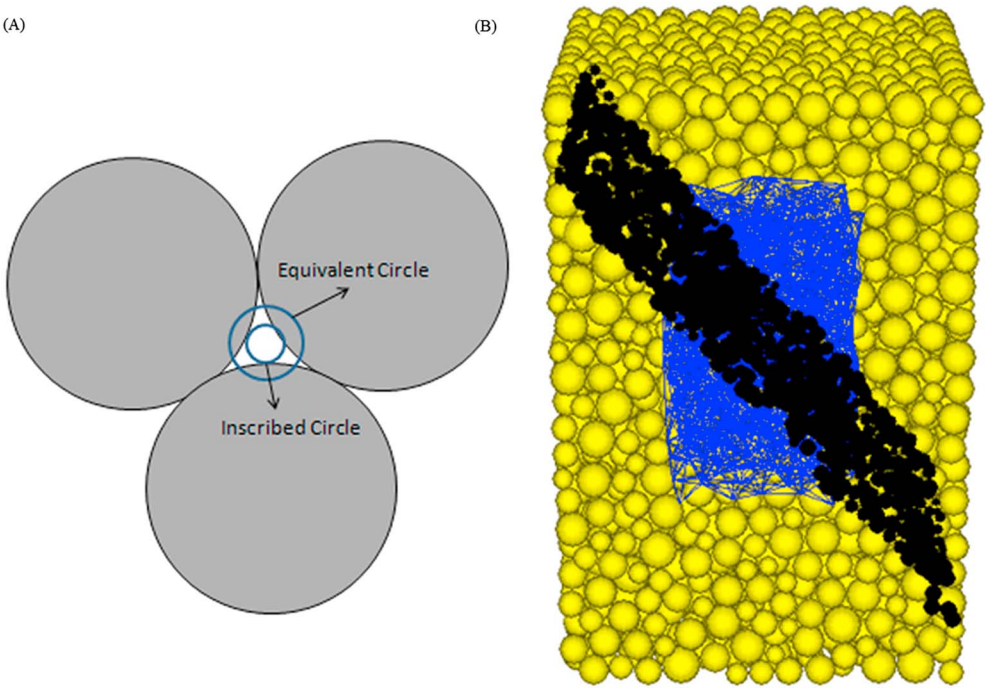

Figure 1. (a) Schematic of circles for calculation of pipes effective radius. (b) Joint plane and pore network in the Berea sample.

where N is number of grains involved in making an event, F_i^k is the ith component of unbalanced force concentrated in the center of Kth grain, and R_j^k is the jth component of distance between contact point and center of kth grain. To interpret the induced seismicity, the moment tensor is decomposed and the source mechanism is displayed in a source-type plot, Hudson diagram [*Hudson et al.*, 1989].

Equal area source-type plot provides graphical presentation of source mechanism of events. The Hudson diagram, as a source-type plot, shows the opening and closure of tensile fractures as well as shearing of fractures. Double couple mechanism represents pure shear displacement along the fracture plane with zero volumetric component at the source map to the center of the diagram. Explosion and implosion type represents pure volumetric change at source map at the top and bottom of the diagram. Mechanisms correspond to the opening and closing of cracks map to top right and bottom left of Hudson diagram. By applying Hudson diagram, a variety of source mechanisms involved in fracture deformation could be distinguished.

2.4. Construction of a Fractured Berea Sample

In this letter, we demonstrate the usefulness of our approach by building a Berea sample through assigning a uniform grain size distribution of particles with an average grain radius of 0.13 mm [*Zhu and Wong*, 1997]. Packing and cementation of grains are simulated by a material genesis procedure [*Potyondy and Cundall*, 2004] to make the initial distribution of grains packed yield an initial porosity of 21% [*Zhu and Wong*, 1997]. We find appropriate micromechanical properties of the modeled sample by comparing the mechanical response of a synthetic sample in the numerical triaxial test to the response of the rock measured in laboratory. The micromechanical properties assigned to simulate mechanical behavior of Berea sandstone are shown in Table 1. The model is calibrated using published experimental rock mechanical data of Berea sandstone [*Zhu and Wong*, 1997]. A Berea specimen with dimensions 3 mm × 4.5 mm × 3 mm is constructed. The geomechanical domain in the sample is larger than the fluid flow domain, and the pore network is only built at the center of geomechanical domain to avoid large computation time associated with the pore network. Smooth joint contact model is applied to simulate smooth interface between grains and to model discontinuities [*Mas Ivars et al.*, 2008]. In this method, orientation of contacts between particles is neglected to model joint without considering roughness of interface. By applying this method, particles do not move around each other; instead, they slide along each other and experience shearing in the smooth frictional surface.

Table 1. Properties of the Berea Sandstone Sample

Berea's Properties	
Grain distribution	Uniform grain size
Grain density(kg/m^3)	2650
Inter-grain friction	0.4
Microscale Young modulus(GPa)	5.25
Normal/Tangential stiffness	2
R_{ave}(mm)	0.13
R_{max}/R_{min}	1.85
Grain number	6505
Intergranular mean tensile strength(MPa)	55
Intergranular mean shear strength(MPa)	55
Normal strength deviation(MPa)	15
Shear strength deviation(MPa)	15
Peak strength at 5 Mpa	85
Young Modulus at 5 MPa	5
Permeability(Darcy)	0.348
Sample porosity	0.21

3. Results and Discussion

A smooth fracture is applied to the Berea sample with a dip angle of 45° and dip direction of 0°, shown in Figure 1b. The joint particles have the same stiffness as that of intact particles and have the microstrength of one fifth of intact grains. We performed a numerical triaxial test under confining pressure of 5 MPa, shown in Figure 2a, to study the effect of deformation of plane fracture on transport and seismic source behavior of the sample, shown in Figures 2b and 3c. Due to application of axial load, the sample is compacted before losing its strength and the size of the pore structure decreases as well. After reaching the peak strength, the rock experiences expansion. This expansion of the rock is mainly due to shearing along the fracture plane, which causes enhancement of the sample permeability. The mechanism of AE events during deformation of plane fracture is concentrated in the middle of DC and closure of cracks shown in Hudson diagram, proving presence of negative volumetric component in the source of AE events, shown in Figure 3c. We performed the same numerical triaxial test on the fractured samples with different roughness to study how transport and seismic source responses change inside the fractured rock as a function of fracture properties.

3.1. Effect of Dilation Angles

Dilation angle represents the volumetric expansion of rock materials during its failure. Dilation of fracture could be modeled indirectly by assigning dilation angle in the smooth joint model. To consider dilation of the fracture in the smooth joint model, we added dilation angle to the parameter list of the grains that make the joint. Based on the amount of shear deformation in the grains on the joint plane, we are able to apply normal displacements on the grains as a function of assigned grain dilation angle. Dilation of fracture could be modeled directly by considering grains roughness along the joint in the natural joint model. To study the real dilation of the Berea sample, we applied a natural joint to the intact Berea sample as well with the same orientation and micromechanical properties of the smooth joint, already studied in this work. Then, we investigate its effect on mechanical behavior of the Berea sandstone sample. In this approach to represent a discontinuity, roughness, and bumpiness of particles on either side of the joint will affect its mechanical behavior, such as its peak strength and dilation, naturally. As shown in Figure 2a, the sample with natural joint has lower peak strength in comparison to the intact sample due to the lower microstrength of grains

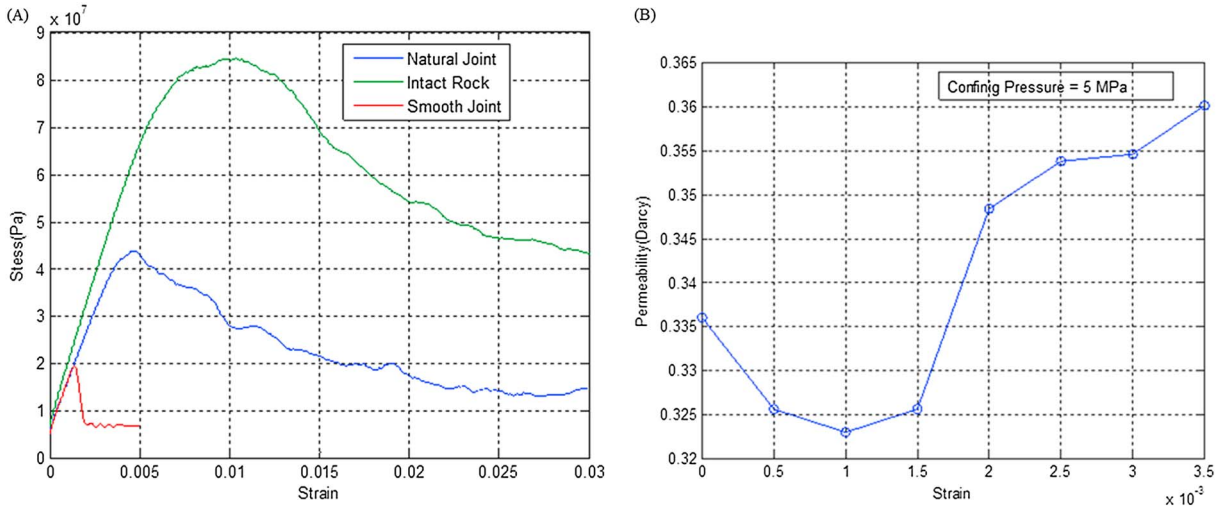

Figure 2. (a) Effect of smooth and natural joint on mechanical behavior of sample. (b) Effect of smooth joint on transport properties of sample.

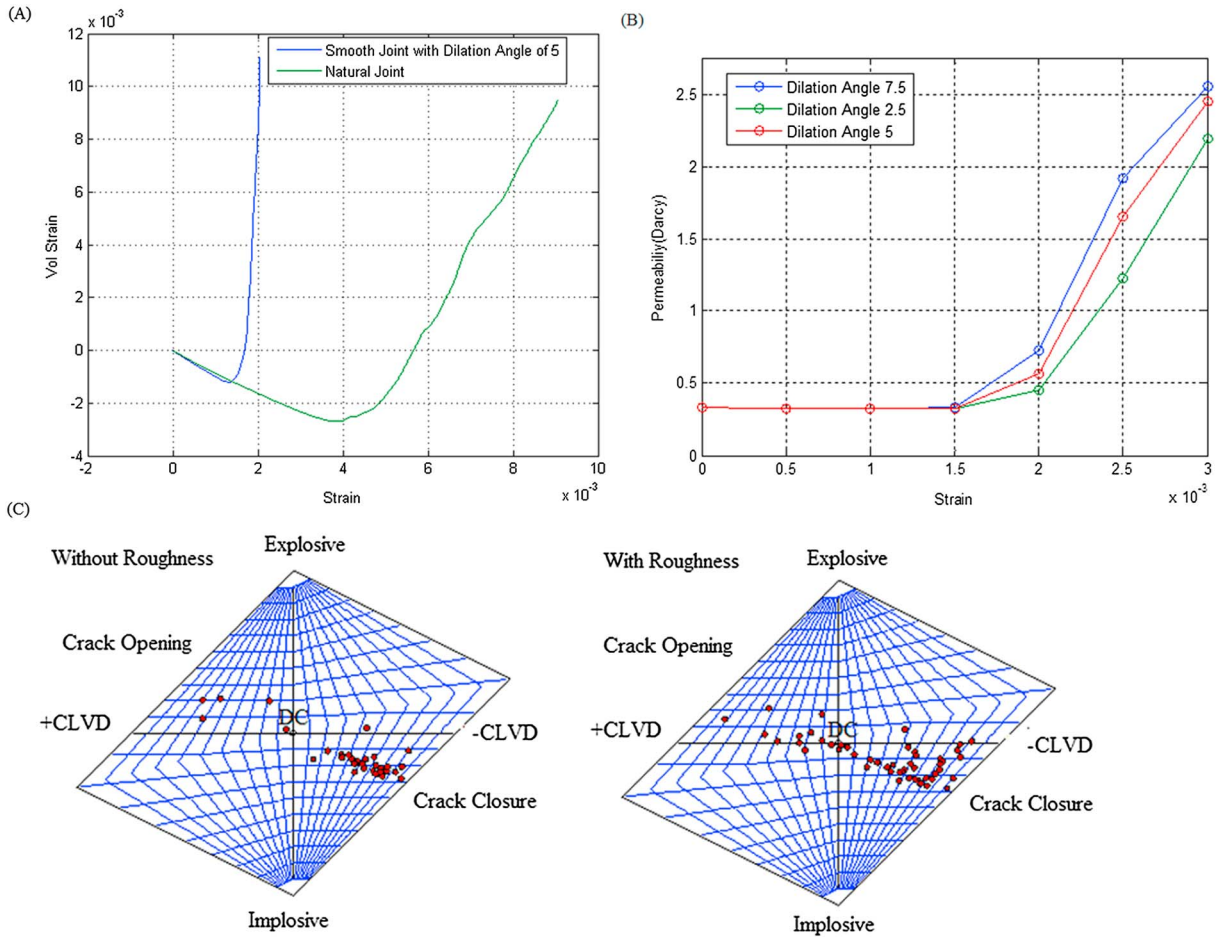

Figure 3. (a) Volumetric deformation of sample with natural and smooth joint. (b) Effect of dilation angle on transport properties of sample. (c) Effect of dilation angle on source mechanism of AE events plotted in Hudson diagram.

along the joint. On the other hand, it has higher peak strength in comparison to the sample with the smooth joint due to considering the effect of roughness of joint. We made a comparison between volumetric expansion of sample with natural joint and sample with smooth joint having dilation angle of 5°, Figure 3a. In both cases, after movement of the fracture plane by applying shear force to it, the volume of the sample increases. Although the failure of sample with smooth joint occurs at lower strain, the amounts of volumetric deformation of both samples after failure are near to each other. The variation of dilation angle in the fractured sample with the smooth joint sample is chosen around this value.

The models with different dilation angles have nearly the same peak strength, and the main impact of applying dilation angle occurs during the shearing of the fracture. Effect of rock deformation on the permeability of the fractured sample is shown in Figure 3b. Due to shearing of the fracture surface, the pipes radii in the updated pore network increase inside the sample and enhance the permeability. The total expansion of the rock is significantly higher in the case of fractured samples with a higher dilation angle that results in larger permeability of sample, as shown in Figure 3b. The source mechanism of AE events in the sample after shearing of fractures is shown in Figure 3c under confining pressure of 5 MPa. In the case with zero dilation angle, the source mechanism of AE events are concentrated in the middle of DC and closure of cracks. By applying dilation angle to the joint particles, the source mechanism of AE events shows more disperse behavior and move toward opening of cracks. This proves that roughness of the fracture, represented by dilation angle, could generate tensile forces in the source of failure resulting in deviation of source mechanism of acoustic emission events toward opening tensile part and enhances the permeability of the sample significantly during its failure under confining pressure.

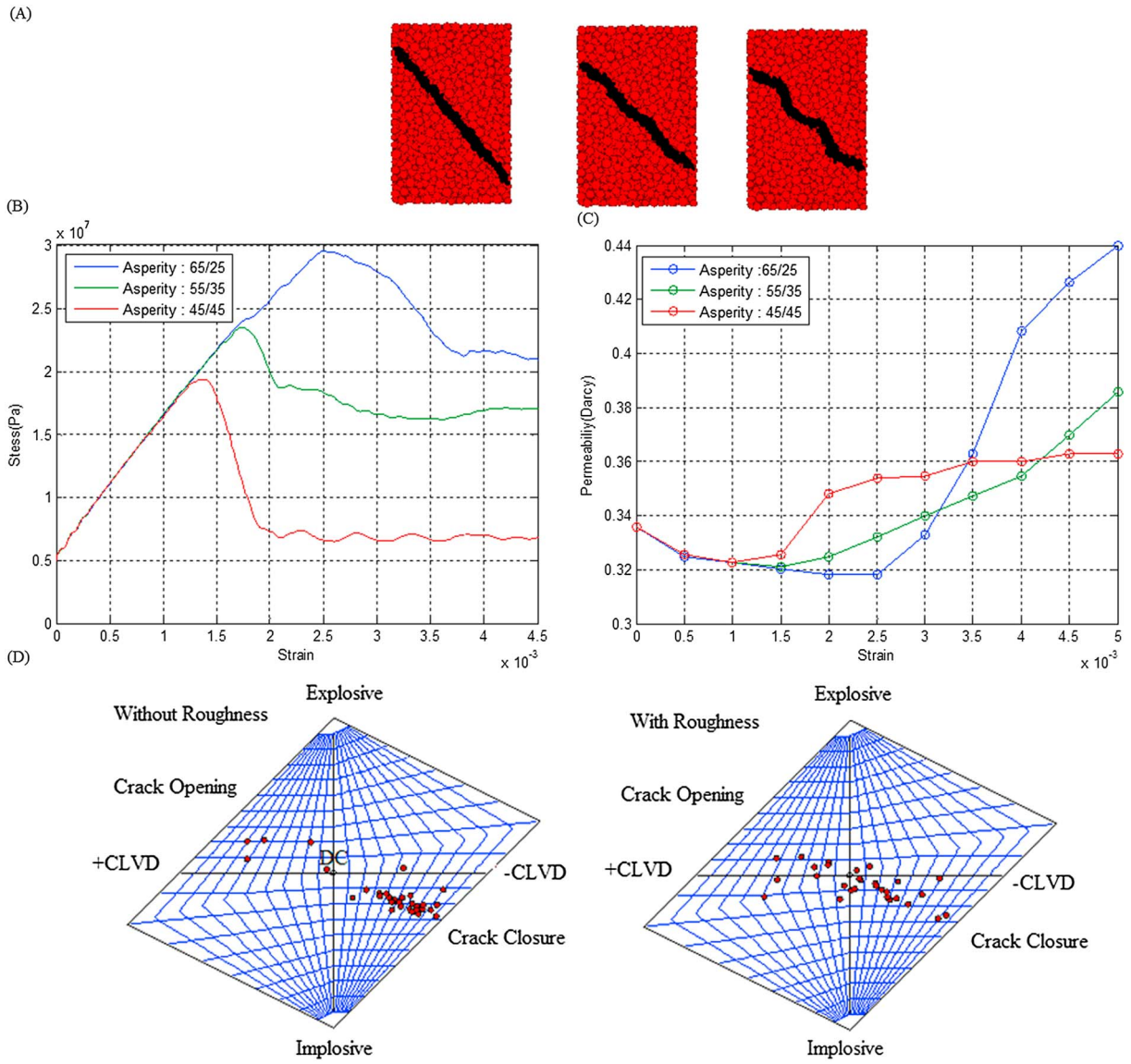

Figure 4. (a) Asperities with deviation of 10 and 20° applied to the plane joint. (b) Effect of joint asperities on mechanical behavior of sample. (c) Effect of joint asperities on transport behavior of sample. (d) Effect of joint asperities on source mechanism of AE events plotted in Hudson diagram.

3.2. Effect of Asperity of Fracture

To study the effect of asperity of fractures on mechanical behavior, i.e., deformation and peak strength of a fractured sample, a deviation of 10 and 20° from original dip angle of fracture is applied to the different parts of the plane joint. A schematic of the fractured sample with two different asperity angles is shown in Figure 4a. Its effect on mechanical and fluid flow properties of the fractured sample is shown in Figures 4b and 4c. By presence of asperity on the fracture, the fracture becomes rougher. Both peak and residual strength of sample is a function of asperity angle. In fact, the asperity resist shearing along the fracture, leading to higher strength of the sample. By applying higher deviation of asperity angles, the peak strength of the sample increases and occurs at higher strain. In addition, the residual stress of the sample is increased leading to higher sample dilation. The fluid flow and seismic source response of fractured samples follow its mechanical behavior. The permeability is higher after shearing of fractures in the case of sample with a rough fracture due to larger natural dilation of sample after rock deformation. By increasing the asperity angle, this effect is more pronounced and lead to more increment of permeability of the sample. By further shear deformation, degradation of asperity may happen, affecting its dilation. In our work, the asperity is as strong as in intact rock. Our model does not consider damage evolution of the asperities and gouge

generation which may lead to reduction of permeability. The dilation of fracture shows its effect on seismic source mechanism of AE events in Figure 4d. In the case of rough fracture, AE source mechanism deviates from concentrated zone in the plane fracture and shows its tendency toward opening crack part of Hudson diagram. Asperity of the fracture could generate tensile force during its deformation leading to opening of the microcracks and permeability enhancement.

Hydraulic stimulation of geological formations in oil and gas fields or geothermal reservoirs could lead to induced microseismicity. Spatial mapping of the microseismic events enables imaging of the pattern of activated fracture networks that in turn enhances the prediction of fluid flow in subsurface formation [*Baig and Urbancic*, 2010]. Activation of natural fractures could happen under confining pressure, which resist enhancement of permeability. The result of analyzing source mechanism of AE events during failure of rough fracture in our work proves that tensile component in the source of failure can be induced because of fracture surface properties, i.e., its roughness. In addition, the fracture roughness can lead to permeability enhancement in the natural fractures under confining pressure. Changes in permeability of activated fractures in the stimulated reservoir volume correlate with significant improvement in well productivity [*Cipolla et al.*, 2011]. Based on our study on evolution of transport behavior of sample with rough fracture, the roughness of fracture surface could dilate fracture and increase the aperture normal to the fracture surface under confining pressure. Fracture roughness could resist against sliding back of fracture to the initial position, and it could be the main source of fracture permanent dilation when the closure stress is applied after hydraulic stimulation.

4. Conclusions

By applying the hydromechanical-seismic modeling, we are able to study seismic source mechanism and transport behavior of deformed fractured rock samples and the connection between them as a function of fracture properties. Roughness of fracture, leading to shear dilation and aperture variation, was modeled to show its greatest influence on permeability increment and deviation of source mechanism of AE events toward crack opening in the sample. While the AE events generated during deformation of plane fractures have volumetric component toward crack closure and the permeability of a fractured sample could be increased insignificantly, the AE events generated during deformation of rougher fractures have volumetric component toward tensile crack opening, and the permeability of a fractured sample could be increased significantly during its failure, when performing the same triaxial compression test.

Acknowledgments

Support of the University of Wyoming (UW) and UW School of Energy Resources is gratefully acknowledged.

The Editor thanks Christian Huber and an anonymous reviewer for their assistance in evaluating this paper.

References

Aki, K., and P. G. Richards (2002), *Quantitative Seismology*, University Science Books, Sausalito, USA.

Baig, A., and T. Urbancic (2010), Microseismic moment tensors: A path to understanding frac growth, *Leading Edge*, *29*(3), 320–324.

Bryant, S. L., P. R. King, and D. W. Mellor (1993), Network model evaluation of permeability and spatial correlation in a real random sphere packing, *Transp. Porous Media*, *11*(1), 53–70.

Cipolla, C., T. Fitzpatrick, M. Williams, and U. Ganguly (2011), Seismic-to-simulation for unconventional reservoir development, paper SPE 146876 presented at the SPE Reservoir Characterization and Simulation Conference and Exhibition, Abu Dhabi, UAE, 9-11 Oct.

Fischer, T., and A. Guest (2011), Shear and tensile earthquakes caused by fluid injection, *Geophys. Res. Lett.*, *38*, L05307, doi:10.1029/2010GL045447.

Hazzard, J. F., and R. P. Young (2002), Moment tensors and micromechanical models, *Tectonophysics*, *356*(1), 181–197.

Hudson, J., R. Pearce, and R. Rogers (1989), Source type plot for inversion of the moment tensor, *J. Geophys. Res.*, *94*(B1), 765–774.

Julian, B. R., G. R. Foulger, F. C. Monastero, and S. Bjornstad (2010), Imaging hydraulic fractures in a geothermal reservoir, *Geophys. Res. Lett.*, *37*, L07305, doi:10.1029/2009GL040933.

Lockner, D., J. Byerlee, V. Kuksenko, A. Ponomarev, and A. Sidorin (1991), Quasi-static fault growth and shear fracture energy in granite, *Nature*, *350*(6313), 39–42.

Mas Ivars, D., D. Potyondy, M. Pierce, and P. Cundall (2008), The smooth-joint contact model, *Proceedings of WCCM8-ECCOMAS,* Venice, Italy.

Miller, A. D., G. Foulger, and B. R. Julian (1998), Non-double-couple earthquakes 2. observations, *Rev. Geophys.*, *36*(4), 551–568.

Potyondy, D., and P. Cundall (2004), A bonded-particle model for rock, *Int. J. Rock Mech. Min. Sci.*, *41*(8), 1329–1364.

Šílenỳ, J., D. P. Hill, L. Eisner, and F. H. Cornet (2009), Non–double-couple mechanisms of microearthquakes induced by hydraulic fracturing, *J. Geophys. Res.*, *114*, B08307, doi:10.1029/2008JB005987.

Zhu, W., and T.-F. Wong (1997), The transition from brittle faulting to cataclastic flow: Permeability evolution, *J. Geophys. Res.*, *102*(B2), 3027–3041.